Chapter 7:
Estimation of Regional-scale Fluxes of Heat, Water Vapour and Carbon Dioxide

Chapter Contents

7.1 Introduction

Regional-scale estimates of the fluxes of water vapour, sensible heat and CO_2 are required for several reasons.

First, surface-atmosphere exchanges are the main pathways by which water and CO_2 are cycled between the stores at the surface and in the atmosphere, their magnitude is a measure of the rate at which such cycling occurs and their sign indicates the direction of the transfer. Understanding how and why the fluxes vary over the landscape will lead to an improved understanding of the water and CO_2 budgets, allowing better informed management of natural resources (Cleugh et al., 2004).

Second, current estimates of trace gas emissions are based on inventory methods (AGO, 2001). These are bottom-up methods where an emission factor is assumed for a particular process, the prevalence of that process is estimated and the total contribution calculated from the two. Regional-scale estimates of trace gas fluxes can lead to improvements in the emission factors and act as a constraint on the inventory estimates (Galbally et al., 1992; Leuning et al., 2004), particularly for trace gases such as CH_4 and N_2O. In the case of CO_2, regional-scale estimates of F_C will contribute to estimation of the net ecosystem exchange (NEE) of the Australian biosphere. This is only partially addressed by current inventory methods (AGO, 2002) and there is considerable uncertainty in the size, direction and controlling factors of this exchange (Roxburgh, 2001; Chen et al., 2003; Wang and McGregor, 2003).

Third, the last two decades have seen a steady increase in the use of modelling as a tool for investigating surface-atmosphere exchange at the patch (Wang and Leuning, 1998; Leuning et al., 1998; Chen et al., 1999b; Zhan and Kustas, 2001) and global scales (Sellers et al., 1996a). The two approaches have traditionally operated at different extremes of spatial scale but they have converged toward regional scales as computational power has increased. With both approaches, there is a need for estimates of model parameters and validation of model outputs at regional scales. These needs are usually met by extrapolation of point measurements but would be better served by direct estimates of the regional-scale fluxes.

Four techniques have emerged as favoured methods for estimating the regional-scale fluxes of latent heat, sensible heat and CO_2. The most established is a network of micrometeorological towers. This is common to all previous experiments and its logical extension, the establishment of a global network of such stations, is being realised (Baldocchi et al., 2001). Regional-scale fluxes are then calculated as the average over the available sites but the estimates can be biased if the sites are not uniformly distributed (Kelly et al., 1992). Dense networks of ground-based observations are also expensive to implement and careful calibration and intercomparison of instruments is required to ensure the data from all sites are compatible. Their main advantage is that they are able to provide observations throughout the day for extended periods of time.

Instrumented aircraft have been used to provide estimates of the regional-scale fluxes in many field experiments (Desjardins et al., 1992b; Oncley et al., 1997; Said et al., 1997; Samuelsson and Tjernstrom, 1999; Isaac et al., 2004b). Their advantage is that aircraft are able to cover areas of the order of 1000 km^2 on time scales that are short compared to the diurnal cycle but they under-sample a particular surface. Isaac et al. (2004b) also show that aircraft observations are susceptible to short term imbalances in the surface energy budget. Flux observations from aircraft have also been dogged by perceptions of bias based on a lack of agreement between aircraft and ground-based data. However, the results presented in Chapter Four show that excellent agreement can be obtained between aircraft and ground-based observations of F_E and F_H when the data are corrected for differences in the source areas and the effects of sensor response time.

The third approach that has been used to provide estimates of the regional-scale fluxes is a group of methods collectively known as atmospheric boundary layer (ABL) budget techniques. Cleugh et al. (2004) identify three distinct methods within this grouping, the atmospheric boundary layer (ABL) profile approach, the coupled CBL-surface energy balance (SEB) approach and the integral CBL budget approach and discuss their relative strengths and weaknesses. The ABL profile approach (Brutsaert and Mawdsley, 1976) uses measurements of scalar (θ and q) profiles throughout the boundary layer and estimates the surface fluxes from these using

empirical flux-gradient relationships formulated in terms of z_i/L. The CBL-SEB approach (McNaughton and Spriggs, 1986) couples a predictive model of the surface fluxes, usually the Penman-Monteith equation, to a model for the growth of the mixed layer to provide values of the temperature and water vapour concentration in the mixed layer, θ_m and q_m. These are used, along with the externally specified available energy, to predict the fluxes at the next time step and so on throughout the day. Regional values for the aerodynamic and surface conductances must also be specified. The CBL budget approach (Betts and Ball, 1994) inverts the previous method and uses the time evolution of mixed layer scalar concentration to infer the surface fluxes. All of these budget methods suffer from problems, particularly the neglect of horizontal advection and the difficulty in specifying entrainment at the interface between the mixed layer and the free troposphere. In addition to these, the area over which the fluxes are averaged is not explicit and changes throughout the day as the boundary layer evolves. Despite their shortcomings, budget techniques remain the only alternative to inventory estimates for emissions of trace gases such as CH_4 (Denmead et al., 2000) and N_2O (Griffith et al., 2002).

The fourth approach to estimating regional-scale fluxes is the use of coupled meteorological-SVAT (soil-vegetation-atmosphere transport) models (Sellers et al., 1996a; Martin et al., 1999; Finkele et al., 2003). These modelling approaches cover a wide range in spatial and temporal resolutions as well as a wide range in the sophistication with which canopy and soil process are described. Typically, the mean meteorological fields from a GCM or a mesoscale model are used to drive a model of surface-atmosphere exchange and, in on-line simulations, the resulting predictions of F_E and F_H are fed back into the meteorological model. A common theme across all approaches, though, is that increasing sophistication is matched by an increasing number of soil and canopy parameters that must be specified but this does not always result in better performance (Pitman and Henderson-Sellers, 1998). Wang and Leuning (1998) describe a simple model of photosynthesis and energy partitioning that still requires seven parameters to be specified. A subsequent analysis in Wang et al. (2001) concludes that only three or four of these parameters can be reliably estimated from micrometeorological observations. Remote sensing is

another possible source of data from which model parameters can be estimated. However, current efforts have largely been limited to the use of empirical relationships to estimate leaf area index (L_{ai}), the fraction of vegetation cover, the fraction of absorbed photosynthetically active radiation ($fPAR$) from $NDVI$ (Sellers et al., 1996b; Myneni et al., 2002). The problem of specifying the necessary parameters, particularly those averaged over the appropriate horizontal scale, continues to complicate the use of coupled meteorological-SVAT models. A variation of the coupled meteorological-SVAT model uses inversion techniques to infer large-scale fluxes from trace gas concentrations and air trajectories. Wang and Barrett (2003) and Wang and McGregor (2003) describe the application of this method to Australian conditions.

This chapter examines a hybrid technique for estimating the regional-scale fluxes of latent heat, sensible heat and CO_2. It is based on the hypothesis that, over a useful range of scales, the spatial and temporal variations in the surface fluxes are separately contained in the surface properties and meteorological forcing respectively. This separation allows spatially varying surface properties to be used with time-varying meteorology from a central site to calculate surface fluxes over heterogeneous landscapes. The surface properties can be estimated from ground-based and airborne observations and can be extrapolated from point to regional scales on the basis of empirical relationships between the surface properties and $NDVI$. This approach differs from those discussed above in several ways. It avoids issues in scaling from patch to regional scales since the region can be treated as the sum of its patches. The scaling from leaves to canopy or canopy to patch is contained, respectively, in the spatial averaging implicit in the ground-based or airborne observations used to estimate the surface properties. The method provides a link between the canopy and regional scales using the assumptions that the spatial variability in the meteorological forcing is small and that the empirical relationships used to interpolate the surface properties are valid across the region. Finally, the technique provides a method of integrating ground-based observations, modelling and remotely sensed data to estimate regional-scale averages of heat, water and CO_2 exchange.

Section 7.2 presents the models used to estimate the regional-scale fluxes of latent heat, sensible heat and CO_2. The spatial variability of the fluxes and the meteorology used by the models to predict them is examined in Section 7.3 by considering the site to site correlation and the site to site changes in magnitude. Section 7.4 presents the daily averaged values of, and diurnal trend in, F_E, F_H and F_C calculated using the surface property method and compares these predictions to the available observations and published results from a CBL budget technique and a coupled mesoscale-SVAT model. Conclusions are given in Section 7.5.

7.2 Models for Estimating Regional Fluxes

7.2.1 General

Chapter Five introduced four surface properties, the evaporative fraction α_E, the maximum stomatal conductance g_{sx}, the Bowen ratio β and the water-use efficiency W_{UE}, and explored how these quantities varied over the OASIS domain. The relationship between the surface properties and the Normalised Difference Vegetation Index ($NDVI$) was investigated in Chapter Six and was found to be robust enough to allow the interpolation of the surface properties from patch to regional scales using remotely sensed data.

This chapter describes two methods of estimating regional-scale evapotranspiration by combining spatially varying surface properties, α_E and g_{sx}, with meteorology from a central location, in this case the average of the data from the Browning oats and pasture sites. The estimates of F_E are then used to calculate the regional-scale fluxes of sensible heat and CO_2. Sensible heat is calculated as the residual in the surface energy budget (SEB) using the available energy measured at the central location. The CO_2 flux, F_C, is calculated using regional F_E and water-use efficiency, W_{UE}. The required surface properties are estimated from aircraft observations of the fluxes (see Chapter Five) and from $NDVI$ derived from a Landsat image of the OASIS domain (see Chapter Six). Values of the surface properties derived from the aircraft data are used to estimate fluxes for the 10 km by 10 km grid area and for the OASIS transect. Values derived from $NDVI$ are used to estimate fluxes across a region of 130 km by 50 km.

The following sections present the equations used to estimate the regional scale fluxes. The notation is the same as that adopted in Chapter Five with the addition of the superscript g to identify ground-based data.

7.2.2 Simple Ratios

The fluxes of latent and sensible heat at each location k for hour j on day i are calculated using the available energy measured by the ground-based instruments $F^{\mathrm{g}}_{A,ij}$, the evaporative fraction $\langle \alpha_{\mathrm{E}} \rangle_k$ and the assumption of SEB closure:

$$\langle F_E \rangle_{ijk} = \langle \alpha_{\mathrm{E}} \rangle_k F^{\mathrm{g}}_{A,ij} \tag{7.1}$$

$$\langle F_H \rangle_{ijk} = F^{\mathrm{g}}_{A,ij} - \langle F_E \rangle_{ijk} \tag{7.2}$$

Results from the ground-based sites for the diurnal trend in W_{UE} are inconclusive but when averaged over the paired crop and pasture sites at Wagga and Browning, W_{UE} remains within 10% of the daily average value for 5 hours in the middle part of the day. This means that use of an average value of W_{UE} throughout the day will correctly predict daily values of F_C but not its diurnal evolution. The spatially averaged F_C is given by:

$$\langle F_C \rangle_{ijk} = \langle W_{UE} \rangle \langle F_E \rangle_{ijk} / \lambda \tag{7.3}$$

The daily average regional fluxes are then found by averaging over the K locations and the J observing periods during the day:

$$\begin{aligned} \langle F_E \rangle_i &= \frac{1}{J}\frac{1}{K}\sum_{j=1}^{J}\sum_{k=1}^{K}\langle F_E \rangle_{ijk} \\ \langle F_H \rangle_i &= \frac{1}{J}\frac{1}{K}\sum_{j=1}^{J}\sum_{k=1}^{K}\langle F_H \rangle_{ijk} \\ \langle F_C \rangle_i &= \frac{1}{J}\frac{1}{K}\sum_{j=1}^{J}\sum_{k=1}^{K}\langle F_C \rangle_{ijk} \end{aligned} \tag{7.4}$$

7.2.3 Maximum Stomatal Conductance

This section describes the forward technique used to estimate the spatially-averaged latent heat flux $\langle F_E \rangle$ using the maximum stomatal conductance $\langle g_{sx} \rangle_k$, and ground-based observations of $S_{\downarrow}$, D, F_A and G_a.

The time varying, spatially averaged canopy conductance is estimated using:

$$\langle G_c \rangle_{ijk} = \frac{\langle g_{sx} \rangle_k}{c_Q} \ln\left(\frac{S^{\mathrm{g}}_{\downarrow,ij} + S_{50}}{S^{\mathrm{g}}_{\downarrow,ij} \exp\left(-c_Q L_{ai}\right) + S_{50}} \right) \left(\frac{1}{1 + D^{\mathrm{g}}{}_{ij} / D_0} \right) \qquad 7.5$$

Assuming that soil evaporation occurs at the equilibrium rate, the surface conductance can be calculated using:

$$\langle G_s \rangle_{ijk} = \langle G_c \rangle_{ijk} \left(\frac{1 + G^{\mathrm{g}}_{a,ij} / \varepsilon G^{\mathrm{g}}_{i,ij} + \tau G^{\mathrm{g}}_{a,ij} / (\varepsilon + 1) \langle G_c \rangle_{ijk}}{1 + G^{\mathrm{g}}_{a,ij} / \varepsilon G^{\mathrm{g}}_{i,ij} - \tau} \right) \qquad 7.6$$

The diurnal variation of F_E is then calculated using the Penman-Monteith equation, rewritten below with the spatial and temporal dependencies of the various terms made explicit:

$$\langle F_E \rangle_{ijk} = F^{\mathrm{g}}_{\mathrm{A},ij} \left(\frac{\varepsilon + G^{\mathrm{g}}_{a,ij} / G^{\mathrm{g}}_{i,ij}}{\varepsilon + 1 + G^{\mathrm{g}}_{a,ij} / \langle G_s \rangle_{ijk}} \right) \qquad 7.7$$

The fluxes of sensible heat and CO_2 are calculated using Equations 7.2 and 7.3 and daily averages calculated using Equation 7.4. Equations 7.5 to 7.7 will be referred to as the coupled g_{sx}-PM model.

Several assumptions are made in using Equations 7.5 to 7.7. Time averages of $S_{\downarrow}$, F_A and D from the ground-based data are taken as being equivalent to spatial averages, and it is assumed that the Penman-Monteith equation is valid at the regional scale (Raupach, 1991; McNaughton, 1994). Soil evaporation is assumed to occur at the equilibrium rate, which is justified by separate studies using miniature lysimeters at Wagga in 1991 and 1993 which found soil evaporation to be 20% greater than equilibrium evaporation (Leuning et al., 1994). In the absence of similar data for Browning and Urana, which receive less rainfall than Wagga, soil evaporation has been assumed to occur at the equilibrium rate for the whole OASIS transect in 1995. Finally, it is assumed that the meteorological data from the centrally located Browning site are representative of the area over which the estimates of g_{sx} have been derived. The same assumption is required when using the simple ratio method described in the previous section and the validity of this assumption is checked in the following section.

7.3 Spatial Variability of Meteorological Quantities

7.3.1 General

This section examines the spatial variability in the turbulent fluxes of momentum, heat, water vapour and CO_2 and the bulk meteorological quantities of incoming short wave radiation, available energy, saturation deficit and aerodynamic conductance. This is done to test the assertion that the bulk meteorological quantities show relatively little spatial variability compared to the fluxes, this being the companion to the assertion, confirmed in Chapter Five, that the surface properties show relatively little diurnal trend compared to the fluxes. The validity of these two assertions forms the basis for arguing that the spatial and temporal variability of regional scale fluxes are, to a large extent, contained in the surface properties and the meteorology respectively. The bulk meteorological quantities are chosen because they are the input data to the coupled g_{sx}-PM model.

The turbulent fluxes are of interest because regional-scale estimates of these quantities are sought and they may be approximated by measurements at the patch scale when synoptic conditions are steady and the surface is homogeneous. The bulk meteorological quantities are of interest because the fluxes can be calculated from these, with the aid of suitable models, when the surface heterogeneity limits the spatial extrapolation of the fluxes themselves. The spatial variability in the fluxes and the bulk meteorological quantities is assessed by examining the auto-correlation and magnitude of each quantity as functions of increasing separation distance. Leuning et al (2004) examined the spatial coherence in daily averages of F_H and F_E for the 1994 and 1995 OASIS data sets. The analysis in this section goes further to include u_*, F_C and the bulk quantities, as well as investigating the spatial variability in the magnitudes, and uses hourly averages because these are used in Equations 7.1 to 7.7. Daily averages are predominantly affected by changing synoptic conditions whereas hourly averages are predominantly affected by the diurnal cycle.

7.3.2 Correlation Between Sites

Figure 7.1 shows the spatial variation in the auto-correlation coefficient for the turbulent fluxes (u_*, F_H, F_E and F_C) and the bulk meteorological quantities (D, $S_\downarrow$, F_A and G_a). The site pairings used for this analysis were Browning oats to Browning pasture (2 km), Browning to Urana (33 km), Browning to Wagga (53 km) and Wagga to Urana (86 km). Data from the crop and pasture sites at each location were averaged for the Browning to Urana, Browning to Wagga and Wagga to Urana comparisons.

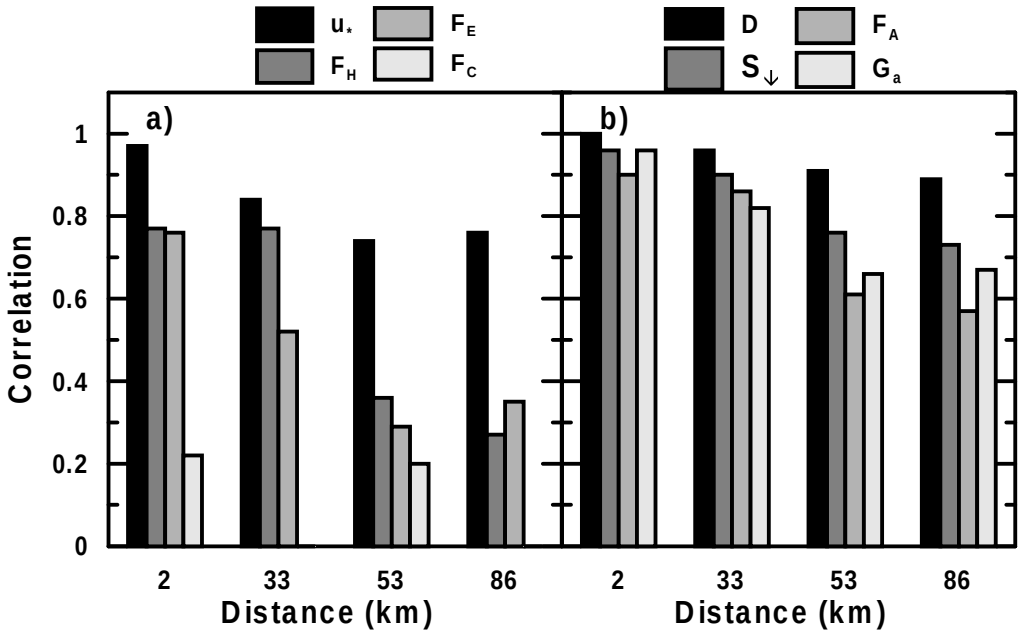

Figure 7.1 The variation of the auto-correlation coefficient as a function of increasing distance from the Browning Oats site for a) the turbulent fluxes and b) the bulk meteorological quantities.

The auto-correlation coefficient for F_E and F_H drops below 0.5 at a separation distance of between 33 and 53 km. This is in agreement with the finding by Leuning et al (2004) that the correlation length scale for F_E was less than 45 km during the 1995 OASIS experiment. It is not possible to estimate the correlation length scale for F_C because of the poor correlation between observations of this quantity at different sites. The correlation coefficient for F_C between crop and pasture sites at Browning ($r^2 = 0.22$, see Figure 7.1) and Wagga ($r^2 = 0.06$, data not shown) are

small despite the small separation distances (2 and 0.3 km respectively). Figure 7.1 also shows that there is little change in the correlation coefficient with increasing distance, from $r^2 = 0.22$ at 2 km (Browning crop versus Browning pasture) to $r^2 = 0.20$ at 53 km (Browning to Wagga). Of the turbulent fluxes, only u_* shows significant correlation along the transect from $r^2 = 0.97$ at 2 km to $r^2 = 0.76$ at 86 km.

The results show that the bulk meteorological quantities maintain significant correlation at separation distances up to 86 km, much further than for F_E, F_H and F_C. The next section considers the variation in magnitude of the turbulent fluxes and the bulk meteorological quantities across the same landscape.

7.3.3 Changes in Magnitude Between Sites

Figure 7.2 shows the diurnal trend in the turbulent fluxes at Wagga, Browning and Urana averaged over the days when data was available at all sites. The fluxes of latent heat, sensible heat and CO_2 all show significant variation along the transect. Peak values of F_E at Wagga are approximately double those at Browning with a further decrease by a factor of two from Browning to Urana. A similar trend occurs for F_H but in the reverse direction (Urana larger than Wagga). CO_2 fluxes at Browning are almost three times smaller than the corresponding values at Wagga.

By comparison, $S_{\downarrow}$, F_A and G_a show much less variation along the transect with variations in peak values of 5%, 27% and 12% respectively, see Figure 7.3. There is a distinct variation in D along the transect with peak values varying from 8.4 g kg^{-1} at Wagga to 14.0 g kg^{-1} at Urana. This is a variation of approximately ±25% about the value of D measured at Browning and is due to the variation in both T_a and q along the transect, see Figure 2.7 in Chapter Two. The effect of spatial variability in D on F_E is limited because stomatal conductance and evapotranspiration have opposite responses to changes in the humidity deficit. This will reduce the impact of the variation in D on F_E predicted by the coupled g_{sx}-PM model.

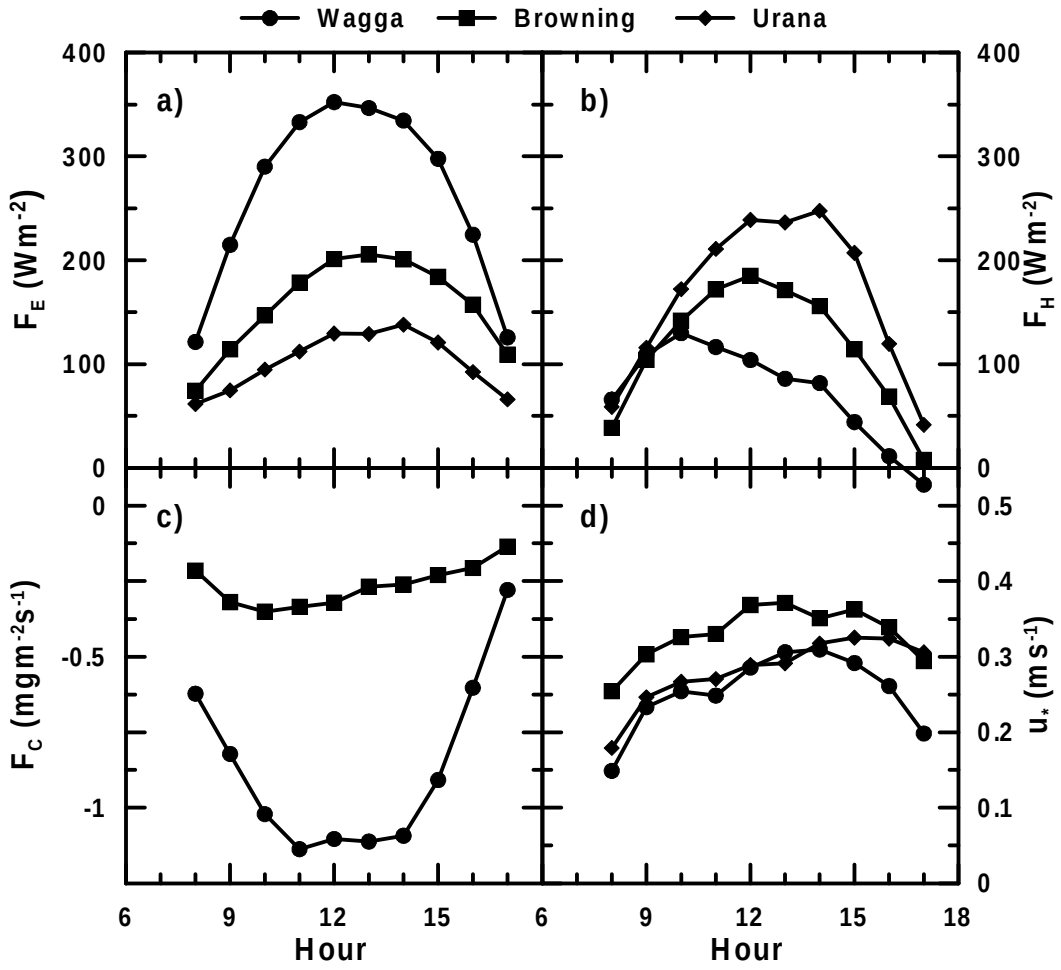

Figure 7.2 Spatial variation of a) F_E, b) F_H, c) F_C and d) u_* along the OASIS transect in October 1995.

Overall, the bulk meteorological quantities show a greater degree of correlation and a smaller change in magnitude from site to site than the fluxes themselves. In particular, the spatial variation in the bulk quantities is much less than their diurnal trend. This complements the finding in Chapter Five that the diurnal trend in the surface properties is much less than their spatial variability. Together these results confirm that the spatial and temporal variability in the regional scale fluxes can be split into the surface properties and the meteorology respectively.

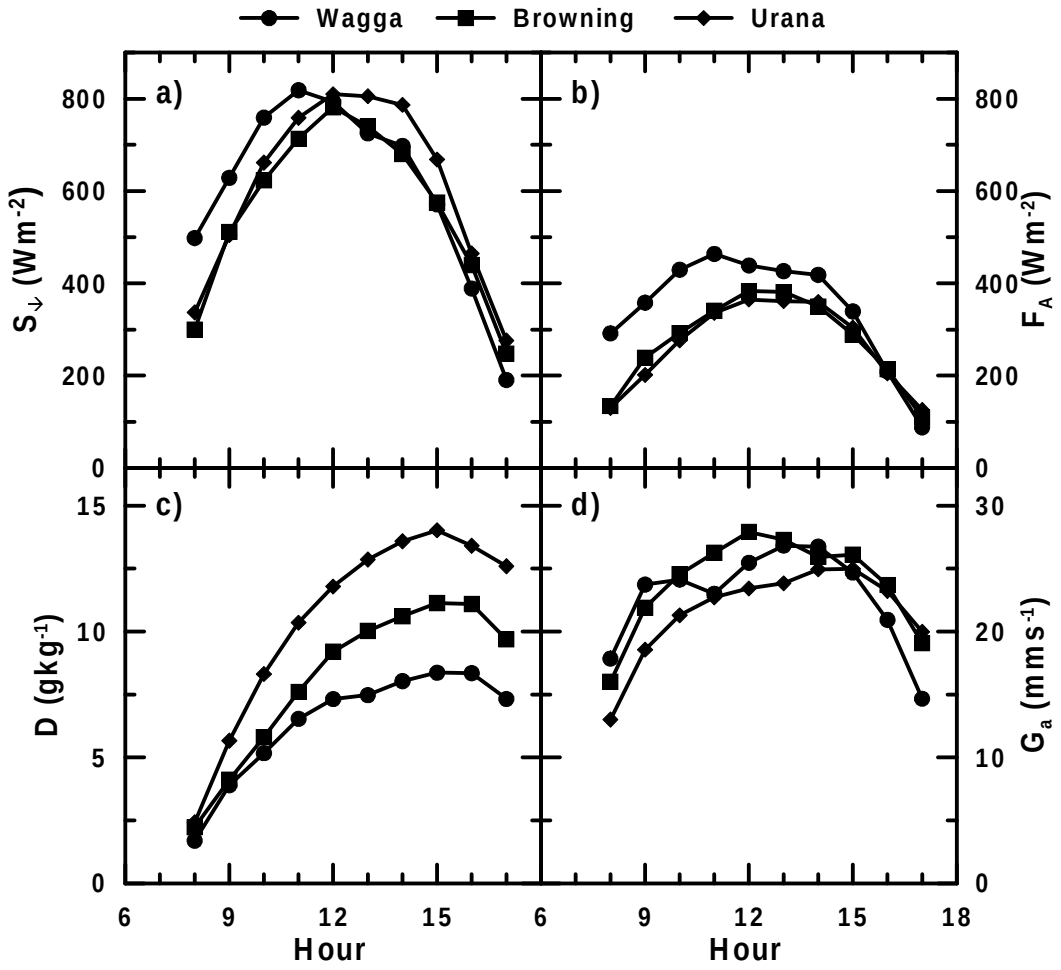

Figure 7.3 Spatial variation of the bulk meteorological quantities of a) $S_{\downarrow}$, b) F_A, c) D and d) G_a along the OASIS transect in October 1995.

The higher spatial coherence and lower spatial variability in the bulk meteorological quantities compared to the fluxes also means that there will be less error in extrapolating the bulk quantities measured at a central location over the OASIS domain than there would be in extrapolating the fluxes. This means that a model that combines surface properties with meteorology measured at a central location is expected to provide more accurate predictions of regional scale fluxes than simply extrapolating the measured fluxes. The results of this approach are examined in the following three sections.

7.4 Results

7.4.1 General

This section describes the results obtained by applying the methods described in Section 7.2 at three different scales using data from the 1995 OASIS experiment. The two smallest scales are the grid area and the transect and at these scales the observed and predicted fluxes can be directly compared in order to validate the surface property approach using values estimated from the aircraft data. The quantities compared are the diurnal trend in the fluxes, averaged over all available days, and the daily average fluxes.

The largest scale is the OASIS domain but the lack of observations at this scale means that there is no data that can be considered as the definitive measurement of the regional scale flux. However, there are four estimates of fluxes available at this scale: from the network of ground-based sites, from the coupled g_{sx}-PM model, from an integral CBL budget (ICBL) technique and from a coupled meteorological-SVAT model. With none of these holding the advantage of obvious truth, the results from all are compared for consistency. For this analysis, the surface properties are estimated from the *NDVI* image of the OASIS domain. At all three scales, the meteorology required is taken from the Browning ground-based sites and only daytime hours, 0800 to 1700 inclusive, are considered.

7.4.2 The OASIS Grid

Average values of α_{E}, g_{sx} and W_{UE} for grid flights on 5 days were calculated from the aircraft data using the methods described in Chapter Five. The spatially averaged surface properties were then used with meteorological data from the Browning site to provide estimates of $\langle F_E \rangle$, $\langle F_H \rangle$ and $\langle F_C \rangle$ for the 10 km by 10 km grid area and these estimates have been compared to the average of the fluxes over the crop and pasture sites at Browning. The model values were calculated by averaging the fluxes predicted using the meteorological data measured at the crop and the pasture sites. Isaac et al (2004b) present results from a similar analysis for F_E only but they use

values of α_E and g_{sx} from each day of grid flights rather than the approach adopted here of averaging the surface properties over all available days.

Figure 7.4a, c and e show the diurnal trend in the observed and predicted fluxes of latent heat, sensible heat and CO_2 averaged over the five days of grid flights. Both the evaporative fraction and the maximum stomatal conductance methods reproduce the diurnal variation in F_E well, though both over-predict F_E in the morning and under-predict F_E in the afternoon, α_E more so than g_{sx}. The diurnal trend in F_H is also well predicted by the two approaches though both over-predict F_H around noon by approximately 15%. Both methods predict the diurnal course of F_C quite well given the assumption that W_{UE} is constant throughout the day.

Figure 7.4b, d and f compare the observed daily average fluxes of F_E, F_H and F_C from the Browning sites with those predicted by the two models for the five days of grid flights, 23 - 27 October inclusive. The comparison statistics are listed in Table 7.1.

Table 7.1 Comparison of the observed and predicted daily averaged F_E, F_H and F_C for the five grid flights. m is the slope of the best fit line through the origin, r^2 is the correlation coefficient, MD is the mean difference and SD is the standard deviation of the difference. Uncertainty in m is the 90% confidence interval.

		m	r^2	MD		SD
F_E	g_{sx}	1.07 ± 0.04	0.53	13	W m^{-2}	13
	α_E	1.09 ± 0.03	0.67	13	W m^{-2}	12
F_H	g_{sx}	0.85 ± 0.03	0.41	-23	W m^{-2}	11
	α_E	0.85 ± 0.02	0.73	-24	W m^{-2}	8
F_C	g_{sx}	1.02 ± 0.25	0.00	-0.04	mg m^{-2} s^{-1}	0.09
	α_E	1.05 ± 0.21	0.00	-0.04	mg m^{-2} s^{-1}	0.08

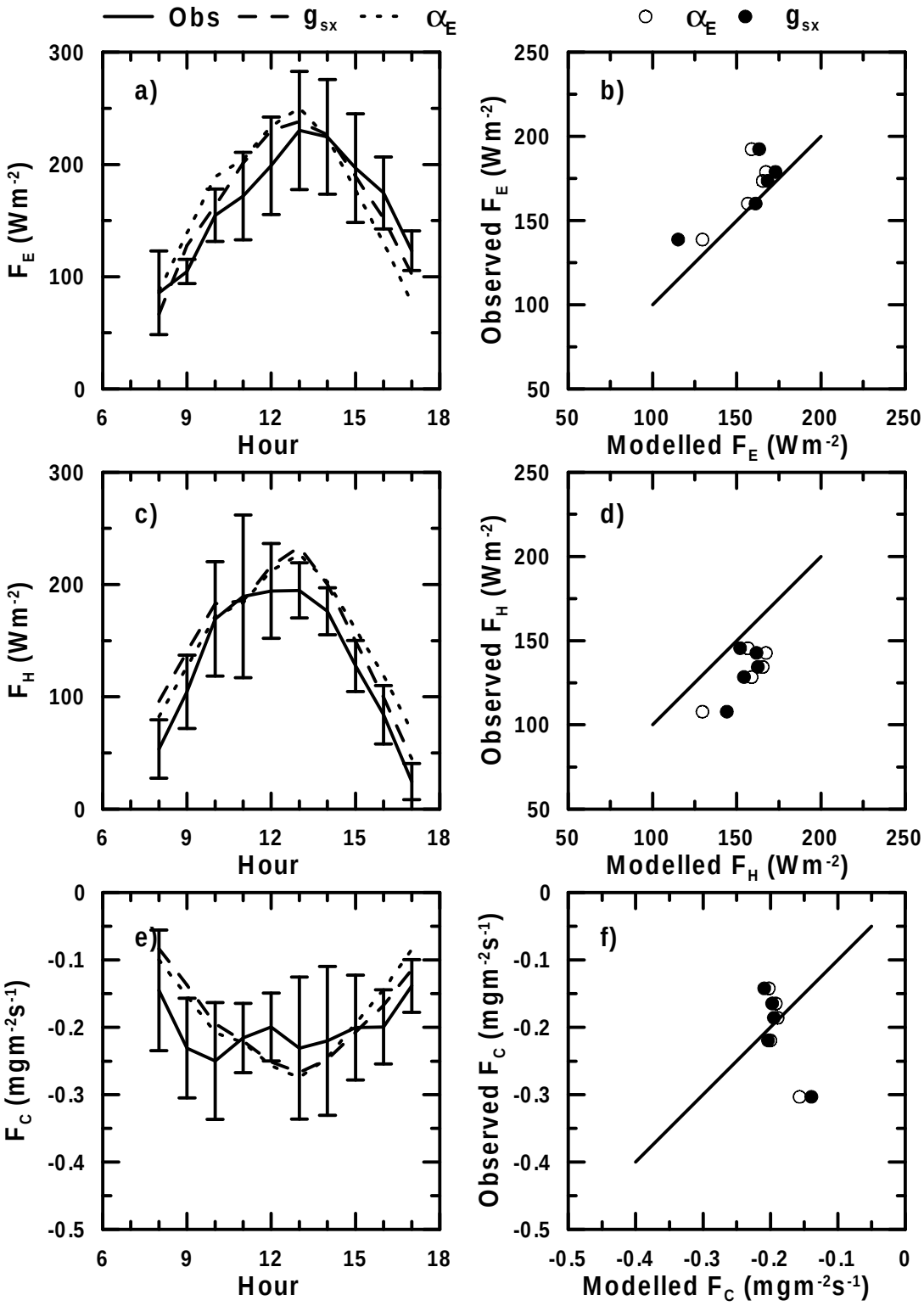

Figure 7.4 Diurnal trend in the observed and modelled a) F_E, c) F_H and e) F_C and comparison of daily average values of b) F_E, d) F_H and f) F_C for the 5 days of grid flights. Error bars on the diurnal trend plots are plus and minus one standard deviation of the observations.

The two models perform well in predicting the daily averaged F_E over the grid area. There is a small positive bias for both the g_{sx} and α_{E} models, and reasonable correlation between the predicted and observed values. The correlation between observed and modelled F_H is also good and both models have a small negative bias. This is expected because F_H is calculated as the residual in the surface energy budget so a tendency to under-predict F_E will result in the over-prediction of F_H. Both models under-predict F_C by 2% and 5% for g_{sx} and α_{E} respectively but there is no correlation between the observed and predicted values.

The results show that both models reproduce the diurnal trend and the day-to-day variation in F_E. This justifies the use of a constant value for α_{E} and g_{sx} through the day and confirms that most of the temporal variation in F_E and F_H is contained in the meteorology. The case for F_C is less clear. The diurnal trend is predicted using a constant value of W_{UE} during the day, but neither model predicts the day-to-day variation. This was not improved by allowing the surface properties to vary from day-to-day.

7.4.3 The OASIS Transect

Average values of α_{E}, g_{sx} and W_{UE} from the aircraft transect segments centred on the ground-based sites were used with meteorological data from the Browning site to estimate the daily averages of and the diurnal variation in F_E, F_H and F_C for the OASIS transect. Observed values of the fluxes were obtained by averaging data from the crop and pasture sites at Wagga, Browning and Urana and these were compared to the values predicted using the surface properties. The extent to which the two estimates agree is a test of the ability of the surface property method, with meteorology measured at a single location, to reproduce the results of the ground-based network, with fluxes measured at several locations. This provides a check of the assertion that the spatial and temporal variability in regional scale fluxes is mostly contained in the surface properties and the meteorology respectively. Isaac et al. (2004b) present results from a similar analysis for F_E only but they used daily

values of α_E and g_{sx} rather than values for the surface properties averaged over all available days of aircraft data.

The diurnal trend in the observed and modelled fluxes is shown in Figure 7.5a, c and e for F_E, F_H and F_C respectively. The surface properties were averaged over the ten days of transect flights and the resulting values used with all 17 days of data from the Browning site. The daily averages are compared in Figure 7.5b, d and f and the comparison statistics are given in Table 7.2.

Table 7.2 Comparison of observed and modelled (α_E and g_{sx}) daily averaged F_E, F_H and F_C for the transect flights. Columns are as for Table 7.1.

		m	r^2	*MD*		*SD*
F_E	g_{sx}	1.15 ± 0.04	0.59	23	W m^{-2}	19
	α_E	1.19 ± 0.06	0.23	30	W m^{-2}	25
F_H	g_{sx}	0.90 ± 0.03	0.86	-15	W m^{-2}	14
	α_E	0.85 ± 0.06	0.60	-23	W m^{-2}	24
F_C	g_{sx}	2.06 ± 0.17	0.00	-0.22	mg m^{-2} s^{-1}	0.09
	α_E	1.93 ± 0.15	0.00	-0.24	mg m^{-2} s^{-1}	0.08

The diurnal trend in the observations of F_E and F_H are reproduced by the model results. The models predict that the maximum F_C occurs in the early afternoon but the observations of F_C peak in the late morning. These results reflect the use of a single value of W_{UE} for all daytime hours, which forces the modelled F_C to peak at the same time as F_E. In reality, Figures 5.3 and 5.4 in Chapter Five show that W_{UE} decreases through the day at Browning and using a time-dependent value for W_{UE} would move the peak in F_C to an earlier time of the day.

The g_{sx} and α_E models under-predict F_E compared to the observations by 15 and 19% respectively and over-predict F_H by 10 and 15% respectively. As before, F_H is calculated as the residual in the surface energy budget and will be over-predicted if F_E is under-predicted. Both models under-predict F_C by a factor of two compared to the observations.

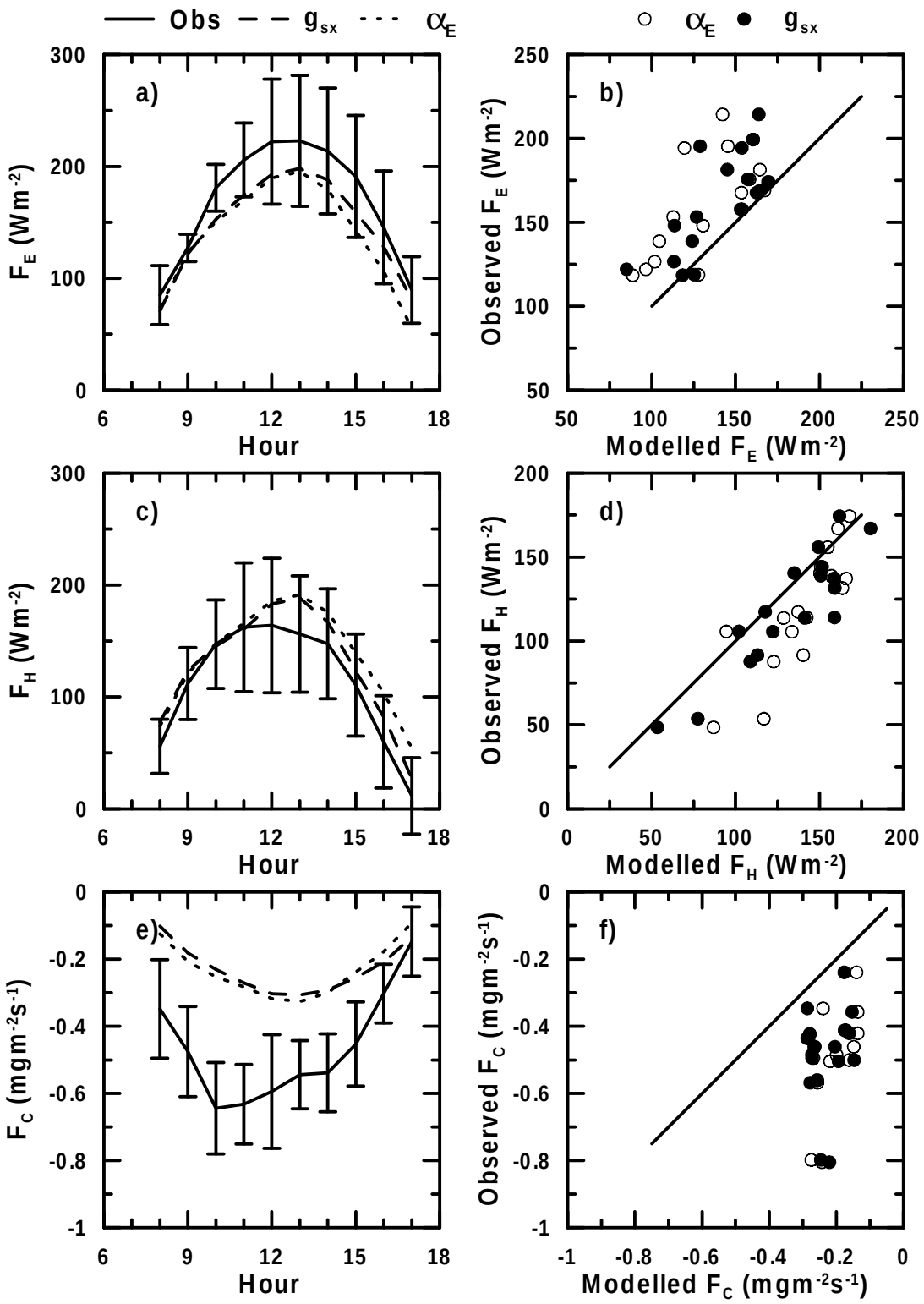

Figure 7.5 Diurnal trend in the observed and modelled a) F_E, c) F_H and e) F_C and comparison of daily average values of b) F_E, d) F_H and f) F_C for the OASIS transect. Error bars on the diurnal trend plots are plus and minus one standard deviation of the observations.

The results show that the surface property method is able to correctly predict the diurnal trend and daily average in F_E and F_H provided the under-prediction of F_E and the over-prediction of F_H can be resolved. The reasons for the bias are best illustrated by comparing the observed and modelled fluxes at each individual site.

Figure 7.6 compares the observed and modelled daily average fluxes at Wagga, Browning and Urana. The observed values are averages of the fluxes over the paired crop and pasture sites at each location for all available days. The modelled values were calculated using g_{sx} derived from aircraft data adjacent to the ground-based sites and bulk meteorological quantities from the Browning sites. The results from the α_{E} model are very similar to those from the coupled g_{sx}-PM model and are not shown.

Figure 7.6 shows that the modelled F_E was consistently less than the observations at Wagga, consistently greater than the observations at Urana and in good agreement with the observations at Browning. The under-prediction of F_E by the coupled g_{sx}-PM model at Wagga is larger than the over-prediction at Urana and this leads to the overall under-prediction seen in Figure 7.5. The reverse pattern is seen in the comparison of observed and modelled F_H because this is calculated as the residual in the surface energy budget. The modelled F_C under-predicts the observations by a factor of two at Wagga but shows good agreement with the observations at Browning after 16 October 1995, the date of the first aircraft flight from which the surface properties were derived. The under-prediction of F_C at Wagga dominates, leading to the overall under-prediction seen in Figure 7.5.

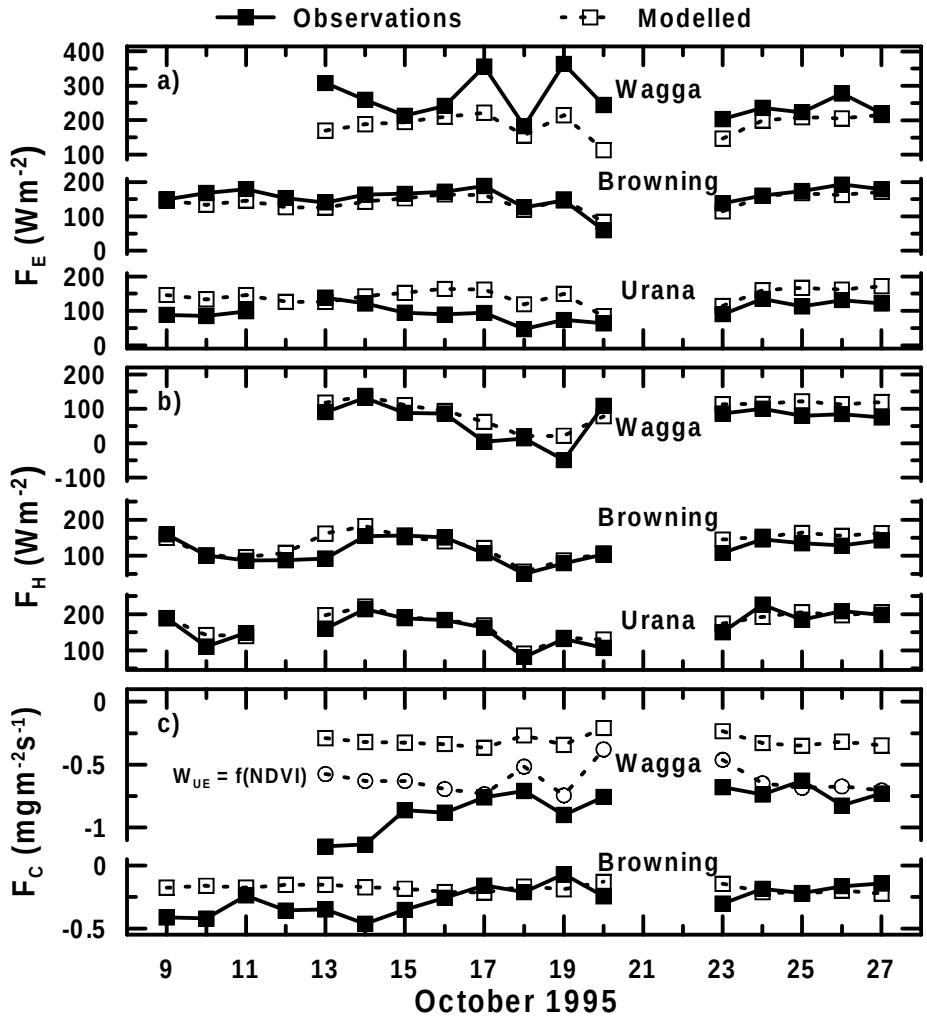

Figure 7.6 Daily average values for a) F_E, b) F_H and c) F_C for the ground-based sites at Wagga, Browning and Urana. Observed values are the average of crop and pasture data, modelled values are predicted using the coupled g_{sx}-PM model. The line in c) labelled $W_{UE} = f\left(NDVI\right)$ shows F_C at Wagga calculated using W_{UE} derived from the average $NDVI$ of the triticale and pasture fields. F_C was not measured at Urana.

The under-prediction of F_E and F_C at Wagga and the over-prediction of F_E at Urana can be traced to differences between the aircraft and ground-based estimates of the surface properties and most of these can be attributed to the disparate source-areas influencing the measurements. This is shown in Table 7.3 where the aircraft and ground-based estimates of the surface properties for each site are listed along with the source-area weighted $NDVI$. The values of α_E, g_{sx} and W_{UE} derived from

the aircraft data are the values used to predict the fluxes shown in Figure 7.5 and Figure 7.6.

Table 7.3 Surface properties and *NDVI* at Wagga, Browning and Urana calculated from the aircraft and ground-based data.

	Wagga		Browning		Urana	
	Aircraft	Ground	Aircraft	Ground	Aircraft	Ground
α_{E}	0.65	0.78	0.55	0.58	0.39	0.38
g_{sx}	11.3	17.5	5.6	6.0	2.7	1.8
W_{UE}	-4.2	-8.2	-3.5	-4.1	-0.8	
NDVI	0.75	0.82	0.73	0.74	0.60	0.62

The aircraft values of α_{E}, g_{sx} and W_{UE} at Wagga are much less than the values obtained from the ground-based data at this site whereas the values are similar at Browning. At Urana, the ground-based and aircraft estimates of α_{E} are similar but the aircraft estimate of g_{sx}, used to predict the fluxes in Figure 7.6, is larger than the ground-based value. The smaller aircraft values for α_{E}, g_{sx} and W_{UE} at Wagga explain the under-prediction of F_E and F_C just as the larger value of g_{sx} at Urana explains the over-prediction of F_E at this site.

The differences between the aircraft and ground-based values of the surface properties at Wagga are due to the different source-areas of the two sets of measurements. This is demonstrated by the values of source-area weighted *NDVI* listed in Table 7.3, which show that the aircraft value is much smaller than the ground-based value. This suggests that the surface influencing the aircraft observations was less photosynthetically active than the area surrounding the Wagga tower and smaller F_E and F_C are expected from the aircraft data. The effect of differences in the source-areas can be estimated by using the relationships developed in Chapter Six to predict the surface property values using the *NDVI* of the ground-based sites. When these values are used to predict the fluxes using the coupled g_{sx}-PM model, the under-estimation of F_E drops from 15% to 10%, the over-estimation of F_H drops from 10% to 7% and the under-estimation of F_C is reduced from a factor of two to only 8%. This is illustrated for F_C at Wagga in Figure 7.6c

where F_C calculated using W_{UE} derived from *NDVI* (open circles) shows much better agreement with the observations than F_C calculated using W_{UE} derived from the aircraft data.

The results for the OASIS transect show that the α_{E} and coupled g_{sx}-PM models reproduce the diurnal trend and day-to-day variation in F_E and F_H. The observed biases in the comparison between the predicted and observed fluxes are substantially reduced when the model values are scaled on the basis of *NDVI* to account for source-area differences, particularly in the case of F_C. This means that the biases are largely an artefact of the locations used in the comparison and do not indicate systematic errors in the α_{E} and coupled g_{sx}-PM models. The following section examines the results obtained by applying the models to the OASIS region using surface properties derived from the Landsat 5 TM image.

7.4.4 The OASIS Domain

This section presents the results of four methods, one observational and three modelling, for estimating regional-scale fluxes of latent heat, sensible heat and CO_2. The observational approach uses the flux measurements at the paired crop and pasture sites at Wagga, Browning and Urana and represents the best estimate of the regional scale fluxes available from the ground-based network. The three modelling techniques are the coupled g_{sx}-PM model, the integral convective boundary layer (ICBL) budget method (Cleugh et al., 2004) and a coupled mesoscale-soil-vegetation-atmosphere-transport (SVAT) model (Finkele et al., 2003). Only F_E and F_H are available from the ICBL and coupled mesoscale-SVAT methods, regional scale estimates of F_C are only available from the ground-based network and the coupled g_{sx}-PM model. The results obtained using the surface property method with α_{E} are almost identical to those from the coupled g_{sx}-PM approach and are not shown.

None of the methods provide definitive values for the regional scale F_E, F_H and F_C because all are subject to significant sources of uncertainty. The ground-based

network consists of only six sites at three locations and the average of the fluxes from these may not equal the true regional scale flux if the sites do not represent the whole OASIS domain. The coupled g_{sx}-PM model has been found to provide accurate predictions of the fluxes at the network sites but this is the first time it has been applied to a larger area. The ICBL technique is subject to errors in the measurement of the scalar profiles and in the estimates of subsidence and horizontal advection. These errors are often hard to identify *a priori* and their presence may only be revealed when the results from this technique are compared to those from alternative methods. The results from the coupled mesoscale-SVAT model are very sensitive to the parameters input to the surface scheme and again, errors in these are hard to identify without recourse to external data for comparison. In the absence of a definitive value for the regional scale fluxes, the results from the four methods are compared and the differences investigated to reveal the shortcomings in a particular approach.

The results compared are the averaged fluxes for daytime hours, 0800 to 1700 inclusive, predicted by the four methods for 9 to 27 October 1995. The observed values are averages of the data from all ground-based sites. The coupled g_{sx}-PM method uses the relationships developed in Chapter Six to interpolate aircraft and ground-based measurements of g_{sx} and W_{UE} over the OASIS domain on the basis of $NDVI$ at a horizontal resolution of 250 m. The interpolated values are then used with meteorology from the Browning site to calculate the regional scale fluxes. The ICBL technique estimates the regional fluxes by integrating profiles of θ and q obtained through the depth of the CBL using instrument packages suspended beneath free-flying balloons. The results from the "full CBL method" described in Cleugh et al. (2004) are used here and referred to as ICBL for simplicity. The coupled mesoscale-SVAT model uses the CSIRO Atmospheric Research limited area prognostic model (DARLAM) to provide the meteorological forcing for the Soil-Canopy-Atmosphere Model (SCAM, Raupach et al., 1997) that predicted the surface fluxes (Finkele et al., 2003). The mesoscale model was run at a horizontal resolution of 30 km and this means that the OASIS transect is represented by the three grid cells

that contain Wagga, Browning and Urana. The results from the coupled mesoscale-SVAT model will be referred to as DARLAM/SCAM.

The results are shown in Figure 7.7 and statistics for the comparison with the observed values are listed in Table 7.4. The use of the observed values does not mean that they are considered to be the best estimate of the regional scale flux, only that they are a convenient reference.

Table 7.4 Comparison of the daily averaged regional-scale F_E, F_H and F_C calculated using three modelling techniques with the average of fluxes observed at Wagga, Browning and Urana. N is the number of points, m and r^2 are the slope and correlation coefficient of the best fit line through the origin respectively, MD is the mean difference and SD is the standard deviation of the difference. See text for a description of the modelling techniques.

	Method	N	m	r^2	MD	SD	Units
$F_E + F_H$	g_{sx}-PM	17	1.03 ± 0.02	0.87	9	17	Wm^{-2}
	ICBL	10	0.97 ± 0.01	0.92	-8	9	Wm^{-2}
	DARLAM/SCAM	17	0.91 ± 0.03	0.51	-26	35	Wm^{-2}
F_E	g_{sx}-PM	17	1.01 ± 0.04	0.30	3	26	Wm^{-2}
	ICBL	10	0.96 ± 0.09	0.00	2	43	Wm^{-2}
	DARLAM/SCAM	17	1.15 ± 0.12	0.00	44	54	Wm^{-2}
F_H	g_{sx}-PM	17	1.03 ± 0.04	0.64	5	21	Wm^{-2}
	ICBL	10	0.95 ± 0.07	0.00	-4	34	Wm^{-2}
	DARLAM/SCAM	17	0.61 ± 0.05	0.00	-70	47	Wm^{-2}
F_C	g_{sx}-PM	17	1.58 ± 0.14	0.00	-0.19	0.16	$mgm^{-2}s^{-1}$
	g_{sx}-PM (sites)	17	1.13 ± 0.10	0.00	-0.07	0.16	$mgm^{-2}s^{-1}$

The sum of the sensible and latent heat fluxes, $F_E + F_H$, from the four methods shows very good agreement. This is expected for the observations, the coupled g_{sx}-PM model and the ICBL method because the latter two use the observed F_A to calculate F_H and F_E, respectively, as residuals in the surface energy budget. However the sum $F_E + F_H$ for DARLAM/SCAM is independent of the micrometeorological data and the close agreement with the observed values means that the model is correctly predicting the available energy. This is a prerequisite for correctly predicting the fluxes.

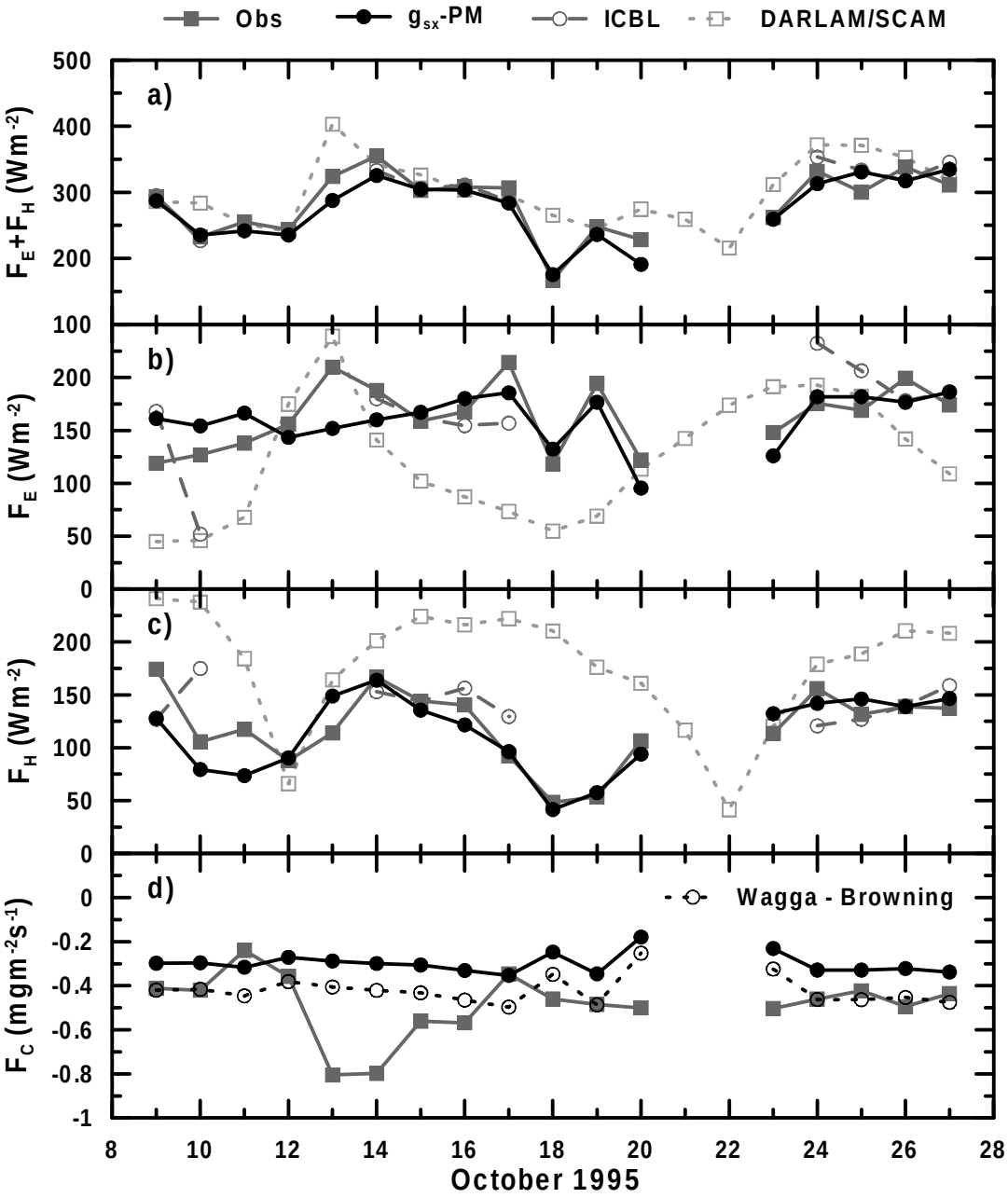

Figure 7.7 Daily average values of a) $F_E + F_H$, b) F_E, c) F_H and d) F_C from the ground-based sites (Obs) and values predicted by the g_{sx}-PM model (g_{sx}-PM), the ICBL budget method (ICBL) and the coupled mesoscale-SVAT model (DARLAM/SCAM). Values for F_C predicted by the g_{sx}-PM model for a subset of the *NDVI* image that corresponds to Wagga and Browning are also plotted in d), see text for details.

There is good agreement between F_E and F_H predicted by the coupled g_{sx}-PM and the observed values though the model tends to under-predict F_E on days when rain

fell (13 October) and when warm air advection was large (17 October). These conditions lie outside the range for which the model was developed. There is good agreement between the observations and the ICBL values on seven out of the ten days for which data from this method is available. The three days of poor agreement occurred when warm air advection was large (10 and 17 October) and immediately after rainfall (24 October). The poor agreement on these days signifies that the assumptions made in applying the ICBL method are not valid in these conditions. The values of F_E and F_H from DARLAM/SCAM are significantly different from the results for the other three methods, even though the sum $F_E + F_H$ shows good agreement. This suggests that the partitioning of available energy at the surface is not being correctly modelled, however results from an offline simulation using SCAM with a more detailed description of the surface type and soil moisture agreed well with the observed fluxes at each site. The implications of this are discussed later in this section.

Regional scale values of F_C are available from the observations and the coupled g_{sx}-PM model. The estimates from the coupled g_{sx}-PM model are consistently smaller than the observations. This is because the observations are averages for the Wagga and Browning sites only but the coupled g_{sx}-PM model results are for the whole OASIS domain. The observations are biased toward larger values because they exclude the areas west of Browning where F_C is small in magnitude and even becomes positive, at the extreme western end of the transect, see Figure 5.7 in Chapter Five. When g_{sx} and W_{UE} are calculated for a restricted area with $NDVI$ between 0.67 to 0.86, the range for Browning pasture to Wagga crop, the bias in the comparison between the observed and modelled F_C drops to 13%. However, F_C calculated using the coupled g_{sx}-PM and W_{UE} does not reproduce the day-to-day variation of the observations.

These results show that the regional scale F_E and F_H predicted by DARLAM/SCAM do not agree with the results from the other three methods. Since $F_E + F_H$ does agree, the reason for the lack of agreement in F_E and F_H is due to the

way the model partitions energy at the surface. This reflects the use by Finkele et al. (2003) of a single surface description with low L_{ai} (1.2) for the three grid cells representing the transect and the use of a spatially invariant soil moisture content to initialise the model. The two day model spin-up, from 7 October 1995 when the simulation began to the first experiment day 9 October 1995, may not have been long enough to allow regional gradients in soil moisture to become established in the model.

The surface area sampled by a ground-based system is of the order of 1 km^2, making the total area sampled by the ground-based network about 6 km^2. The surface area sampled by the aircraft during the transect flights was of the order of 100 km^2. The useable area of the *NDVI* image is 5200 km^2. The good agreement between the regional scale values of F_E and F_H estimated from the ground-based network and those estimated using the *NDVI* image demonstrates that the OASIS sites were representative of the larger domain. Further, the coupled g_{sx}-PM model allows the regional scale, daytime average F_C to be estimated as -0.30 mg m^{-2} s^{-1}, considerably less than the value of -0.49 mg m^{-2} s^{-1} available from the observations. This is because the observations of F_C only represent the eastern half of the OASIS domain and this biases the regional scale F_C estimated from the observations toward the areas of higher rainfall and higher photosynthetic activity.

7.5 Summary and Conclusions

The fluxes of heat, water vapour and CO_2 vary in both space and time across a heterogeneous landscape, forced by the meteorology and modulated by the surface type. This observation prompts two assertions central to the hypothesis of this thesis. First, that over time periods of days to weeks and spatial scales of the order of 100 km, most of the spatial variability in the regional scale fluxes is contained in the surface properties and second, that most of the temporal variability is contained in the meteorology.

The spatial and temporal variability of four surface properties was examined in Chapter Five using aircraft and ground-based data from the 1995 OASIS experiment. The analysis showed that the diurnal trends and day-to-day changes in α_{E}, g_{sx} and W_{UE} were less than the spatial variation. This confirms the first assertion that most of the spatial variability in the regional scale fluxes is contained in the surface properties. This chapter has examined the evidence for the second assertion by comparing the spatial and temporal variability of the bulk quantities D, $S_{\downarrow}$, F_A and G_a and the fluxes F_E, F_H and F_C. It has also explored the use of these surface properties with the meteorology recorded at a central point to predict regional-scale fluxes over the OASIS domain. The predictions have been compared with the available observations and with estimates from a CBL budget technique and a coupled mesoscale-SVAT model.

The results show that values of the bulk meteorological quantities retain their auto-correlation over much larger areas than the fluxes. In addition, there is much less spatial variation in the magnitude of these quantities than there is in the fluxes. This means that the bulk quantities can be extrapolated over a heterogeneous landscape with less error than the fluxes, making them a better choice for extending observations from a sparse network to a region. The small spatial variability in the bulk quantities compared to their diurnal trend confirms the second assertion listed above, that most of the temporal variability in the regional scale fluxes is contained in the meteorology. Together with the results in Chapter Five, this demonstrates that the spatial and temporal variability in the regional scale fluxes of heat, water vapour

and CO_2 can be separated into the surface properties and the meteorology respectively.

The surface property approach to estimating regional scale fluxes has been tested using α_{E}, g_{sx} and W_{UE} derived from aircraft data for the grid and transect flights. Average values of α_{E}, g_{sx} and W_{UE} were combined with the bulk quantities measured at Browning and the predicted fluxes compared with the observations. It is important to note that the observations and the results from the surface property method are not independent and this will tend to enhance their agreement. That said, there is very good agreement between the predicted fluxes and the observations for F_E and F_H. The surface property method under-predicts the observed F_C but this is due to differences in the source-areas of the aircraft measurements, from which the surface properties were derived, and ground-based observations. The under-prediction of F_C reduces to 8% when the surface properties derived from the aircraft data are replaced by values derived from the $NDVI$ of the Wagga site using the relationships developed in Chapter Six. The close agreement between the observed fluxes and values predicted using surface properties at the ground-based sites justifies confidence in the regional scale fluxes estimated by this method.

The results from four methods of estimating regional scale F_E, F_H and F_C were compared to identify the conditions under which they disagreed and hence to gain insight into their relative strengths and weaknesses. For F_E and F_H, the observations and the results from the ICBL and coupled g_{sx}-PM methods are in general agreement, though the results for the ICBL and coupled g_{sx}-PM approaches diverge from the observations on days when the surface is wet and on days of strong warm-air advection. This is because the assumptions used to develop these approaches are not valid in these conditions.

The regional scale F_E and F_H predicted by a coupled mesoscale-SVAT model did not agree with the values from the other three methods, though the sum of the fluxes agreed for all methods. This shows that the coupled mesoscale-SVAT model did not correctly partition the available energy at the surface. This is due to the use of the same surface description for the three grid cells covering Wagga, Browning and

Urana and the initialisation of the model with a spatially invariant soil moisture content. This highlights the difficulty of specifying the inputs to such models with the required accuracy and spatial resolution, especially soil moisture.

Estimates for regional scale F_C are available from the observations at Wagga and Browning and from the coupled g_{sx}-PM model. These agree well when the model is restricted to an area representative of the Wagga and Browning sites. When the coupled g_{sx}-PM model is applied to the whole OASIS domain, the predicted F_C is only 60% of the observed value. This reflects the bias towards the wetter end of the transect due to the lack of F_C measurements at Urana. In this situation, the coupled g_{sx}-PM method is the only one of the four that is able to provide plausible estimates of F_C over the whole of the OASIS domain. The largest uncertainty in the estimates from this method is introduced by the use of a single value of W_{UE} for all days.

Overall, the good agreement between the observations and the results from the coupled g_{sx}-PM model demonstrates that the ground-based network captured most of the heterogeneity of the OASIS domain.

A technique for estimating regional scale fluxes of heat, water vapour and CO_2 has been tested that takes advantage of the natural tendency for the spatial and temporal variability in the fluxes to be contained in the surface properties and the forcing meteorology respectively. The required input data are measurements of bulk meteorological quantities at a site representative of the region, a remote sensing image of the region and a relationship between the remote sensing data and the surface properties. The first two are routinely available and the last poses the biggest challenge to regular application of the technique. However, development of the method allows the focus of inquiry to be sharpened from "How can regional scale fluxes be estimated?" to "How can the relationship between surface properties and remote sensing be specified?". This is a much more specific and tractable task.